

Retrievals of cloud optical depth and effective radius from Thin-Cloud Rotating Shadowband Radiometer measurements

Bangsheng Yin,¹ Qilong Min,¹ Minzheng Duan,² M. J. Bartholomew,³ A. M. Vogelmann,³ and D. D. Turner^{4,5}

Received 2 May 2011; revised 5 October 2011; accepted 5 October 2011; published 13 December 2011.

[1] A Thin-Cloud Rotating Shadowband Radiometer (TCRSR) was developed and deployed in a field test at the Atmospheric Radiation Measurement Climate Research Facility's Southern Great Plains site. The TCRSR measures the forward-scattering lobe of the direct solar beam (i.e., the solar aureole) through an optically thin cloud (optical depth < 8). We applied the retrieval algorithm of Min and Duan (2005) to the TCRSR measurements of the solar aureole to derive simultaneously the cloud optical depth (COD) and cloud drop effective radius (DER), subsequently inferring the cloud liquid-water path (LWP). After careful calibration and preprocessing, our results indicate that the TCRSR is able to retrieve simultaneously these three properties for optically thin water clouds. Colocated instruments, such as the MultiFilter Rotating Shadowband Radiometer (MFRSR), atmospheric emitted radiance interferometer (AERI), and Microwave Radiometer (MWR), are used to evaluate our retrieval results. The relative difference between retrieved CODs from the TCRSR and those from the MFRSR is less than 5%. The distribution of retrieved LWPs from the TCRSR is similar to those from the MWR and AERI. The differences between the TCRSR-based retrieved DERs and those from the AERI are apparent in some time periods, and the uncertainties of the DER retrievals are discussed in detail in this article.

Citation: Yin, B., Q. Min, M. Duan, M. J. Bartholomew, A. M. Vogelmann, and D. D. Turner (2011), Retrievals of cloud optical depth and effective radius from Thin-Cloud Rotating Shadowband Radiometer measurements, *J. Geophys. Res.*, 116, D23208, doi:10.1029/2011JD016192.

1. Introduction

[2] Clouds play a key role in the Earth's climate system because of their critical impact on the atmospheric energy balance and the hydrological cycle. Detailed knowledge of the radiative properties of clouds, such as cloud optical depth (COD), effective radius, and liquid-water path (LWP), is crucial for the study of climate and climate change. To observe accurately these cloud optical properties, various instruments have been developed, such as visible and IR radiometers, microwave radiometers, radars, and lidars. However, they all encounter some limitations when used to retrieve the properties of the optically thin liquid-water clouds [Turner *et al.*, 2007], which are defined here as having LWP less than 100 g/m². For these thin clouds, small uncertainties in the LWP and effective radius can have large

impacts on SW radiative transfer calculations [Min and Duan, 2005]. Therefore, it is important to measure the LWP and effective radius accurately, especially for the low LWP conditions.

[3] To address the need for measuring the LWP of optically thin clouds, Min and Duan [2005] proposed a new multichannel and multiscan radiometer that measures the forward-scattering lobe of the direct solar beam (i.e., the solar aureole) through a thin cloud. On the basis of angular radiance measurements of the solar aureole, the COD and effective radius can be simultaneously retrieved [Min and Duan, 2005]. This technique of using the solar aureole was successfully applied to retrieve the aerosol optical depth and mean radius [Hodkinson, 1966; Nakajima *et al.*, 1983; Kaufman *et al.*, 1994; Dubovik *et al.*, 2000], which is somewhat less challenging than for clouds because the forward scattering for relatively small aerosol particles is not as strong as for the cloud droplets. Recently, DeVore *et al.* [2009] developed an instrument named the Sun and Aureole Measurement, which can measure aureole profiles for thin clouds directly by simultaneously recording the images of the solar disk and solar aureole separately using two cameras. They demonstrated that the COD and cloud drop effective radius (DER) can be derived from the aureole profile.

[4] On the basis of the theory of Min and Duan [2005], researchers at Brookhaven National Laboratory (BNL) developed a Thin-Cloud Rotating Shadowband Radiometer

¹Atmospheric Science Research Center, State University of New York at Albany, Albany, New York, USA.

²Laboratory for Middle Atmosphere and Global Environment Observation, Institute of Atmospheric Physics, Chinese Academy of Sciences, Beijing, China.

³Brookhaven National Laboratory, Upton, New York, USA.

⁴National Severe Storms Laboratory, NOAA, Norman, Oklahoma, USA.

⁵Atmospheric and Oceanic Sciences Department, University of Wisconsin-Madison, Madison, Wisconsin, USA.

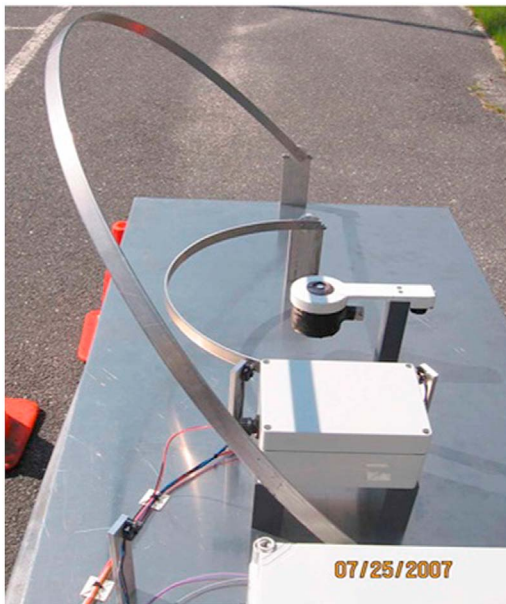


Figure 1. The TCRSR during outdoor testing. The sensor head, located at the center of the image, is occulted alternately by two shadowbands that rotate back and forth over the upper hemisphere. The width of both the bands is 1.8 cm and the radii of rotation for the outer and inner bands are 48.3 and 18.4 cm, respectively, yielding occultation angles of 2.13° and 5.60°. The band rotations are driven by DC motors housed in the white boxes near the center of the image and at the lower right-hand corner. For more design and operation details (see Bartholomew et al., submitted manuscript, 2011).

(TCRSR) by modifying an existing BNL Fast Rotating Shadowband Radiometer to increase the angular resolution of the measurements (M. J. Bartholomew et al., Design of a Shadowband Spectral Radiometer for the retrieval of thin COD, liquid water path, and the effective radius, submitted to the *Journal of Atmospheric and Oceanic Technology*, 2011). The TCRSR is capable of measuring the solar aureole with the shadowband technique and was deployed at the Atmospheric Radiation Measurement Program (Department of Energy, Washington, D. C.) (ARM) Climate Research Facility (ACRF) site at the Southern Great Plains (SGP) [Ackerman and Stokes, 2003]. In this article, we apply the Min and Duan's [2005] retrieval algorithm to the measurements obtained by the TCRSR and evaluate the retrieved cloud properties with other measurements at the ACRF SGP site.

2. The TCRSR and Its Retrieval Algorithm

2.1. TCRSR

[5] The details of the design and operation of the TCRSR are briefly summarized here; for a full description see Bartholomew et al. (submitted manuscript, 2011). The TCRSR is illustrated in Figure 1. A sensor head, located at the center of the instrument, is occulted alternately by two shadowbands that rotate back and forth over the upper hemisphere. The motion of the shadowbands is driven by a DC motor that is controlled by a microcomputer. As a

shadowband passes over the sensor, it blocks a strip of the sky. The instrument is oriented, so that the axis of rotation is parallel to the longitude line at the deployment location. During the sweep, the output from the optical sensor, a Yankee Multifrequency Head, is sampled at a high rate by a 12 bit analog to digital computer (ADC). At the end of a sweep, the ADC data are transmitted to a laptop computer for data processing and storage. In this study, we only use the measurements of the outer band with an occultation angle of 2.13° (hereafter referred to as the 2° band). For the outer band with a smaller occultation angle, the TCRSR is able to measure the forward-scattering radiance closer to the solar disk for more accurate retrievals [Min and Duan, 2005].

[6] For this study, data were obtained at the SGP in July 2008. For the 2° band, a full sweep of 168° took about 14 s, and the sample period was 20 ms. Therefore, a total of 700 samples were collected for each sweep, and the sample spacing was 0.24°. As designed, the motor should rotate the shadowband at a constant speed. However, because of limited motor strength of the prototype and the large shadowband radius, it was possible for the rotating speed of the shadowband to be affected by the torque of its own weight and possibly by strong winds, which would cause errors in blocking-angle registration. Any blocking-angle registration errors will cause uncertainties in the measured shape of the forward-scattering lobe of the solar aureole and consequently impact our retrievals. In this study, we only use the TCRSR measurements from sweeps in one direction, for which the sweeping speed is relatively stable and consistent with the designed value.

[7] The TCRSR measures the angular distribution of light scattered by the clouds in the Sun-sensor direction in six narrow spectral bands. The six spectral bands, each approximately 10 nm wide, are centered at 415, 500, 610, 660, 870, and 940 nm. We used the 415 nm band for the current retrievals, as per Min and Duan [2005], because the surface albedo is low at 415 nm (in the absence of snow cover), and there is little gaseous absorption to interfere with the retrievals.

2.2. Retrieval Algorithm

[8] The blocked radiance b_i at the blocking angle α_i is observed from the scanning measurements of the TCRSR. For a given solar zenith angle α_{sza} , both the cloud droplet effective radius r_e and COD τ can be retrieved by minimizing the following errors [Min and Duan, 2005]:

$$\begin{aligned} e_0 &= b_0 - F_0(\alpha_0, \alpha_{sza}, r_e, \tau) - \exp(-\tau/\cos(\alpha_{sza})) \\ e_i &= b_i - F_i(\alpha_i, \alpha_{sza}, r_e, \tau), \quad i = \pm 1, \pm 2, \dots, \pm m \end{aligned} \quad (1)$$

where $F_i(\alpha_i, \alpha_{sza}, r_e, \tau)$ and e_i are the calculated forward-scattering blocked radiance and error at the i th blocking angle, respectively, as the TCRSR scans across the sky from one side to the other. For the Sun-sensor direction ($\alpha_0 = 0^\circ$), the blocked radiance contains both the attenuated solar beam and forward-scattering component.

[9] To obtain the calculated forward-scattering blocked radiance, $F_i(\alpha_i, \alpha_{sza}, r_e, \tau)$, as given in by Min and Duan [2005], we first compute the radiance field using our fast and accurate 1-D radiative transfer model, which combines the exact radiance of low orders of scattering with the multiple scattering radiance. Then we determine the blocked radiance by applying the shadowband geometry of TCRSR

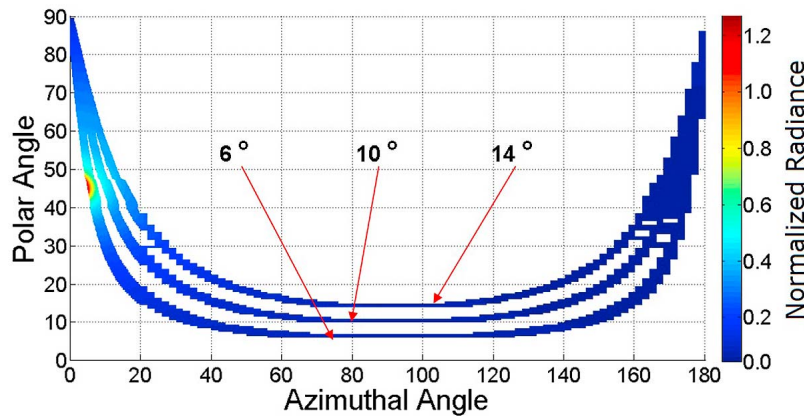


Figure 2. Simulation of the blocked radiance by a 2° shadowband for blocking angles of 6° , 10° , and 14° , for a COD of 1 and a DER of $8 \mu\text{m}$. The solar zenith angle is 45° .

to the simulated radiance field. Figure 2 shows examples of simulations of the radiance blocked by the shadowband for a solar zenith angle of 45° and blocking angles of 6° , 10° , and 14° . To speed up the retrievals, we built a lookup table of the blocked radiances for 64 different CODs, ranging from 0 to 14, 7 different DERs, ranging from 4 to $16 \mu\text{m}$, 16 different solar zenith angles, ranging from 15° to 75° , and different background aerosol optical depths.

3. Measurements and Retrieval

3.1. Calibration and Preprocessing

[10] We evaluate the new instrument and its associated retrieval algorithm via a deployment at the ACRF SGP site, which is well suited for this purpose because it is heavily instrumented to study the clouds and atmospheric radiative transfer. Collocated passive and active radiometric instruments provide concurrent observations of clouds and their geometric and microphysical properties. For the case of 3 July 2008 (shown in Figure 3), the zenith-pointing millimeter-wave cloud radar and standard active remote sensing of cloud layers [Clothiaux *et al.*, 2000] detected a low-level cloud layer with a cirrus cloud layer from 19:30 to 22:30 UTC. The backscatter signal from the micropulse lidar [Spinhirne, 1993] indicated that low-level clouds existed, and the cloud base heights were lower than 2 km. The Microwave Radiometer (MWR) [Liljegren, 1994] detected cloud LWP for the same period (see Figure 7c). As shown by the Total Sky Imager (TSI) and estimated from the direct-beam measurements of the TCRSR, the clouds there were optically thin in the Sun-sensor direction. Together, these data suggest that the period from 19:30 to 22:30 UTC is a good window for testing the TCRSR retrievals. Under further examination, appropriate averaging of the volume depolarization ratio profiles from the Raman lidar [Turner *et al.*, 2002] indicated that the optical depths of the thin ice-cloud layer are less than 0.2 (Figure 3c). The presence of a thin ice cloud over low-level water clouds complicates the TCRSR retrievals. To deal with this situation, we assume a thin ice-cloud layer with an optical depth of 0.15 and an effective radius of $30 \mu\text{m}$ over low-level water clouds in our retrieval algorithm. During periods when there were no apparent low-level clouds, the total optical depth (excluding Rayleigh) was about 0.50, as

determined from the MultiFilter Rotating Shadowband Radiometer (MFRSR) direct-beam measurements [Harrison and Michalsky, 1994]. Therefore, we also assume a background aerosol loading of optical depth 0.35 in our retrieval algorithm.

[11] The TCRSR was calibrated in the laboratory before and after the field experiments; however, the accuracy of a laboratory calibration is only about 4%. At the SGP site, there is also a collocated MFRSR [Harrison *et al.*, 1994] that has been continuously operated at the site for a decade, during which time more than 60 Langley calibrations have been obtained each year. The solar constants obtained from Langley regressions for the spectral bands are interpolated to any particular day using the temporal and spectral analysis procedures of Forgan [1988]. The accuracy of Langley calibration, for a spectral band without gaseous absorption, is within 1%. Therefore, we calibrate the TCRSR measurements against the collocated and well-calibrated MFRSR using the transmission data of the MFRSR to adjust the solar constants used in processing the TCRSR data. As shown in Figure 4, direct-normal and global-hemispheric transmittances are consistent between the MFRSR and TCRSR. However, there are some differences between the two, particularly in direct-normal transmittances. As the two instruments are located 100 m apart, the same cloud can block their direct beams at slightly different times and/or they can observe different parts of the same cloud at a given time. The retrievals from the two instruments would also experience similar time offsets.

[12] A full sweep of the TCRSR takes 14 s, during which time the radiance (and solar aureole) may vary due to changes in the cloud properties and cloud motion. As shown in Figure 5a, the normalized blocked radiance at 22:02 UTC undulates away from the solar aureole region ($>\pm 15^\circ$ around the Sun-sensor direction that occurs at a sweep angle of -46.5°). As shown by Min and Duan [2005], the forward-scattering lobe is concentrated within $\pm 8^\circ$ of the Sun-sensor direction, so we process the raw measurements while focusing on this region. The retrieval algorithm is based on the assumption that the radiance of the attenuated solar beam remains constant during scanning of the shadowband across the solar aureole. The sampling rate of the TCRSR is about 20 ms for 0.24° angular steps; so the sweep time across the

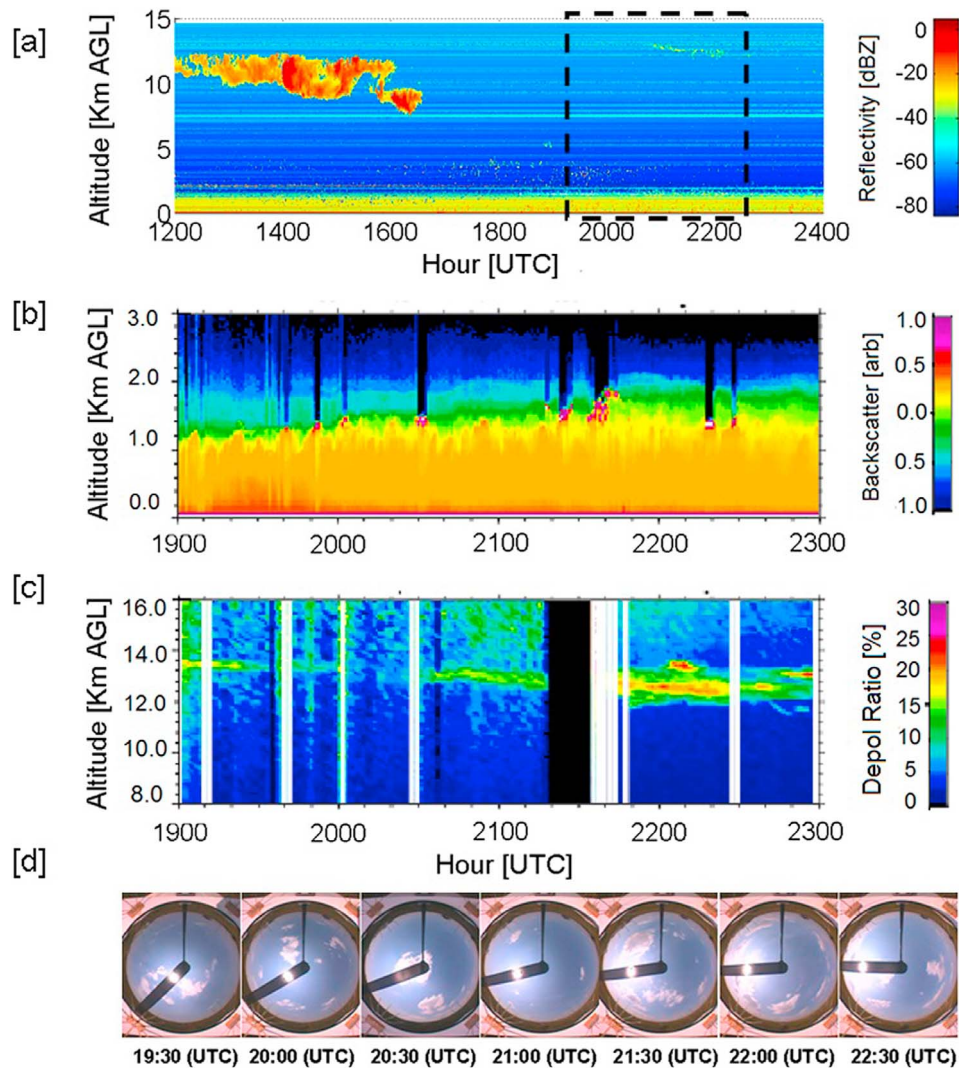


Figure 3. (a) Millimeter-wave cloud radar reflectivity (cirrus mode), (b) attenuated backscatter from the micropulse lidar, (c) volume depolarization ratio from the Raman lidar, and (d) TSI images on 3 July 2008.

solar aureole region ($\pm 8^\circ$) is about 1.5 s. For most situations, it is reasonable to assume that cloud properties are quasi-constant during 1.5 s. Certainly, if a small broken cloud or a cloud edge happens to pass through the direct beam at the time the shadowband is sweeping the aureole, the quasi-constant assumption is violated and would result in retrieval errors.

[13] An expanded view of the solar aureole region in Figure 5a is given in Figure 5b, which shows that the shoulders of the solar aureole are not symmetric. To reduce the potential impact on retrieval error, a second normalization is applied to the TCRSR sweeping measurements, that is, a linear fit between the two shoulders. It is equivalent to assuming that the cloud properties vary linearly within 1.5 s. Because the blocked radiance is obtained by differencing two large values (unshadowed irradiance minus shadowed irradiance), noise in the TCRSR measurements causes an error in determining the shoulders of the solar aureole. Therefore, a high-order polynomial is fit to the raw TCRSR measurements to smooth the noise in the shoulders of the solar aureole. As we only use the relative magnitude and shape of the solar aureole for the retrieval, the polynomial fit and

linear baseline normalization do not affect it. The final fitted line, shown in Figure 5b as the normalized blocked radiance, is the input to the retrieval algorithm.

3.2. Retrievals and Evaluation

[14] By applying the retrieval algorithm to the pre-processed TCRSR measurements, the cloud DER and optical depth are obtained simultaneously. Figure 6a shows the retrieval results for the measurements at 21:27 UTC on 3 July 2008. As illustrated by the TSI image, there was a cloud in the Sun-sensor direction. It is clear that the pre-processed solar aureole from the TCRSR measurements is well matched with the retrieved results, where the latter is the simulated angular distribution of radiance in the retrieval algorithm. The retrieved COD and DER are 0.52 and 7.8 μm , respectively. In comparison, the modeled blocked solar aureole and the measurements in a clear-sky period at 19:59 UTC are shown in Figure 6b, in which the background aerosol optical depth was about 0.48. It is clear that the shoulders of the solar aureole are flatter in the clear-sky period than in the thin-cloud period.

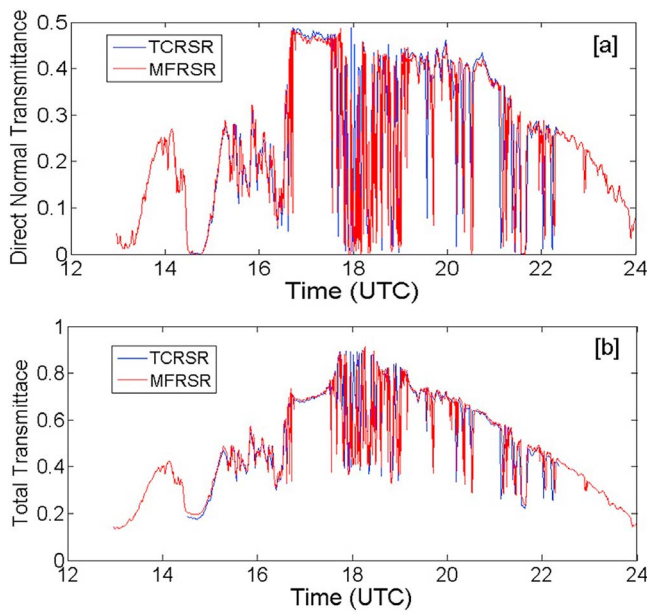


Figure 4. (a and b) Comparisons between TCRSR and MFRSR observed direct-normal and global-hemispheric transmittances on 3 July 2008.

[15] There were no other direct measurements of COD and effective radius along the Sun-sensor direction at the ARM SGP site to which we could compare our results, which reinforces the benefit of developing the TCRSR. To evaluate our retrievals, we compiled all the relevant information at the site from the MFRSR, a zenith-pointing MWR, and a zenith-pointing atmospheric emitted radiance interferometer (AERI) [Knutson *et al.*, 2004a, 2004b]. The COD is retrieved along the Sun-sensor direction from the direct-beam measurements

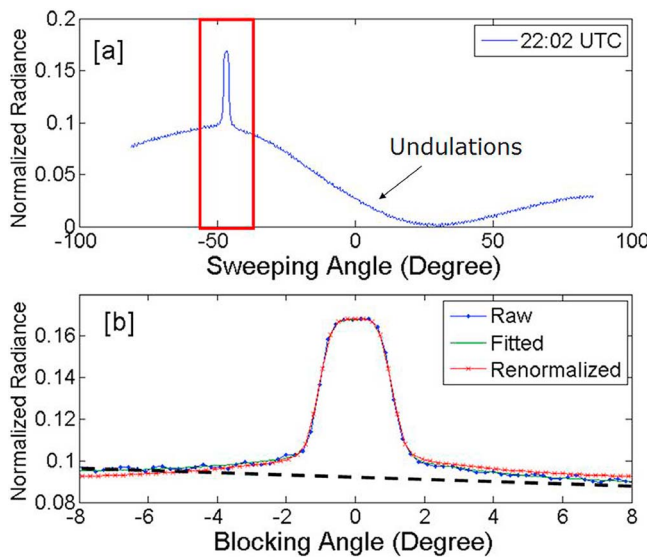


Figure 5. (a) Normalized blocked radiance for the 2° band of the TCRSR during a sweep at 22:02 UTC, 3 July 2008. (b) Expanded view around the solar aureole, showing the raw, fitted, and renormalized blocked radiance. The dashed line is a linear fit to the shoulders of the solar aureole.

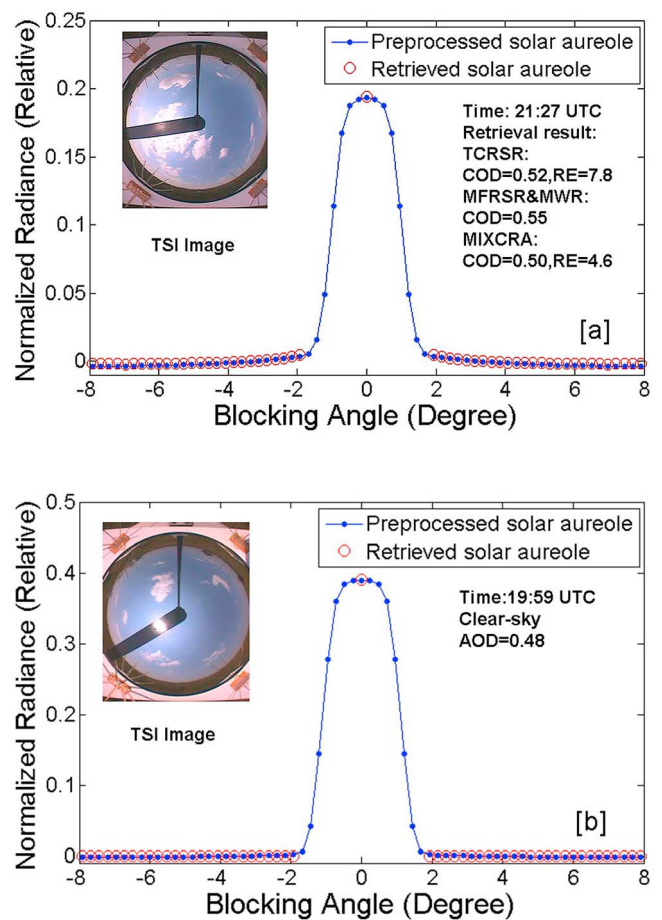


Figure 6. Comparisons between the preprocessed solar aureole from TCRSR measurements (blue dots) and the retrieved solar aureole (red circles) for (a) thin cloud period at 21:27 UTC and (b) clear-sky period at 19:59 UTC.

of the MFRSR by assuming a cloud effective radius of $8 \mu\text{m}$, with an uncertainty less than 5% [Min and Harrison, 1996; Min *et al.*, 2004]. The cloud effective radius and LWP overhead can be determined from the AERI radiances using the mixed-phase cloud retrieval algorithm (MIXCRA) when the optical depth is less than 50 g/m^2 , with uncertainties of $0.4 \mu\text{m}$ and 1.8 g/m^2 , respectively [Turner, 2007]. The LWP overhead can also be measured by the MWR, with an uncertainty of $20\text{--}30 \text{ g/m}^2$ [Marchand *et al.*, 2003]. For the 21:27 UTC period, the CODs retrieved from the MFRSR and MIXCRA measurements are 0.52 and 0.50, respectively, which are close to the TCRSR retrieval. The retrieved effective radius from the MIXCRA is $4.6 \mu\text{m}$, which is smaller than the TCRSR retrieval.

[16] Comparisons of the retrieved COD, cloud DER, and cloud LWP for different periods at the SGP on 3 July 2008 are shown in Figure 7. The LWP retrieved from the TCRSR is calculated as $\text{LWP} = 2/3\pi r_e$. As the TCRSR is calibrated by the colocated MFRSR, the relative difference between the TCRSR-based retrieved optical depths and those from the MFRSR is small (within 5%, see Figure 7a). There are some temporal shifts and magnitude differences between the TCRSR and MFRSR. As discussed previously, they are most likely due to the spatial separation of the two instruments.

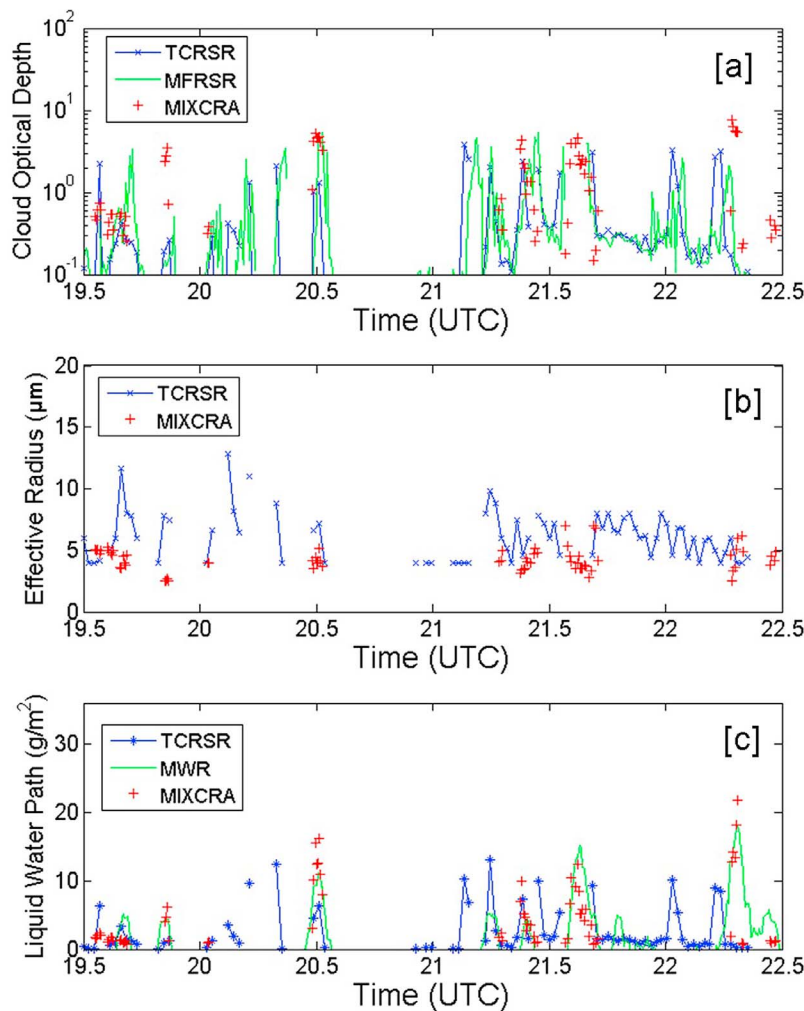


Figure 7. Comparison of (a) COD, (b) DER, and (c) LWP inferred from the TCRSR, MFRSR, AERI, and MWR measurements on 3 July 2008 at the ACRF SGP site.

[17] Because of the differences in the view geometry and/or the field of view of the TCRSR, AERI, and MWR, direct comparison of retrieved effective radius and LWP among these instruments is problematic. Nonetheless, the results in Figures 7b and 7c suggest that the effective radii inferred from the TCRSR are close to or larger than the retrievals from the MIXCRA, and the LWPs inferred from the TCRSR are generally close to those from the MWR and MIXCRA when they are available.

3.3. Error Analysis and Sensitivity Studies

[18] As shown in Figures 7b and 7c, there are some differences in the LWPs and DERs between the TCRSR retrievals and those from the other instruments, requiring further understanding of uncertainties associated with the TCRSR measurements and retrievals. The uncertainty of radiometric calibration has a limited impact on the cloud DERs retrievals for the TCRSR because we applied a transferable Langley calibration with an accuracy of 1% and we normalized the radiance of the forward-scattering lobe. The accuracy of the measured solar aureole shape is sensitive to the accuracy of two key parameters: The occultation angle of the shadowband and the stability of the rotating speed of

the shadowband (i.e., the registration accuracy of the blocking angle). For example, the occultation angle of the TCRSR was originally designed to be 2.00° , but ended up at 2.13° . To illustrate the sensitivity to this difference, we retrieve all the three parameters, COD, DER, and LWP, assuming an occultation angle of 2.00° . Also, a sweep-by-sweep assessment of blocking-angle registration during the field deployment suggested that the DC motor rotation speed may be underestimated by 1.8%. Therefore, we also conduct a sensitivity study by adjusting the sample angular spacing to be 0.244° . As shown in Figure 8, both changes tend to reduce the retrieved DER by $0.6 \mu\text{m}$ for a narrower shadowband and by $0.9 \mu\text{m}$ for a faster-rotating speed.

[19] Because the view-geometry differences of the three retrievals based on the TCRSR, MWR, and AERI result in temporal and spatial mismatches for direct comparison, probability distributions are a good way for quantitative evaluation. The distributions of COD, shown in Figure 9a, illustrate that COD inferred from the TCRSR is systematically smaller than that from MIXCRA. The mean COD from the TCRSR is 0.65, which is smaller than the value of 1.83 inferred from the MIXCRA and is consistent with the value of 0.62 inferred from the MFRSR. In contrast to COD, the

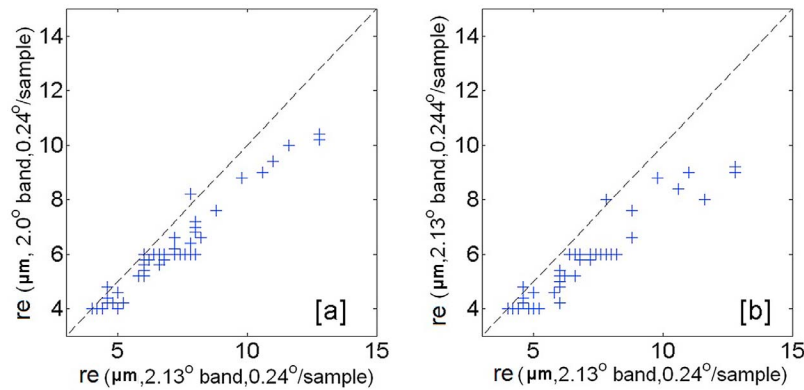


Figure 8. Comparison of the cloud DER retrieved with (a) a narrower shadowband and (b) a fast-rotating speed against the baseline configuration on 3 July 2008.

distribution of cloud DER inferred from the TCRSR is relatively broader than that from the MIXCRA. The mean cloud DER inferred from the TCRSR is $6.1 \mu\text{m}$, which is much larger than the mean value of $4.3 \mu\text{m}$ derived from the MIXCRA. As shown in Figure 9c, all the distributions of LWP from these three instruments show that most clouds have very low LWPs ($\text{LWP} < 5 \text{ g/m}^2$), and that the distribution from the TCRSR is close to that from the MWR. The percentage of lowest LWPs (around 2 g/m^2) from the TCRSR is lower than that from the MWR, but higher than that from the MIXCRA. As shown in Figure 9d, the distributions of the LWP for the two sensitivity tests do not change much. This suggests that the changes in retrieved COD due to the

forward scattering into the direct beam compensate for changes in the cloud DER, the combination of which results in LWP retrievals that are less sensitive to measurement uncertainties.

[20] As discussed previously, this case is complicated because of the presence of a thin ice-cloud layer that overlies the low-level water clouds. Moreover, the optical properties of the upper-level ice-cloud layer and the background aerosol varied with time and were hard to measure precisely from the current instrument suite at the site, especially when the low-level clouds were present in the instruments' fields of view. Therefore, the retrieval results are affected by the background aerosol and ice-cloud optical properties including (1) the size

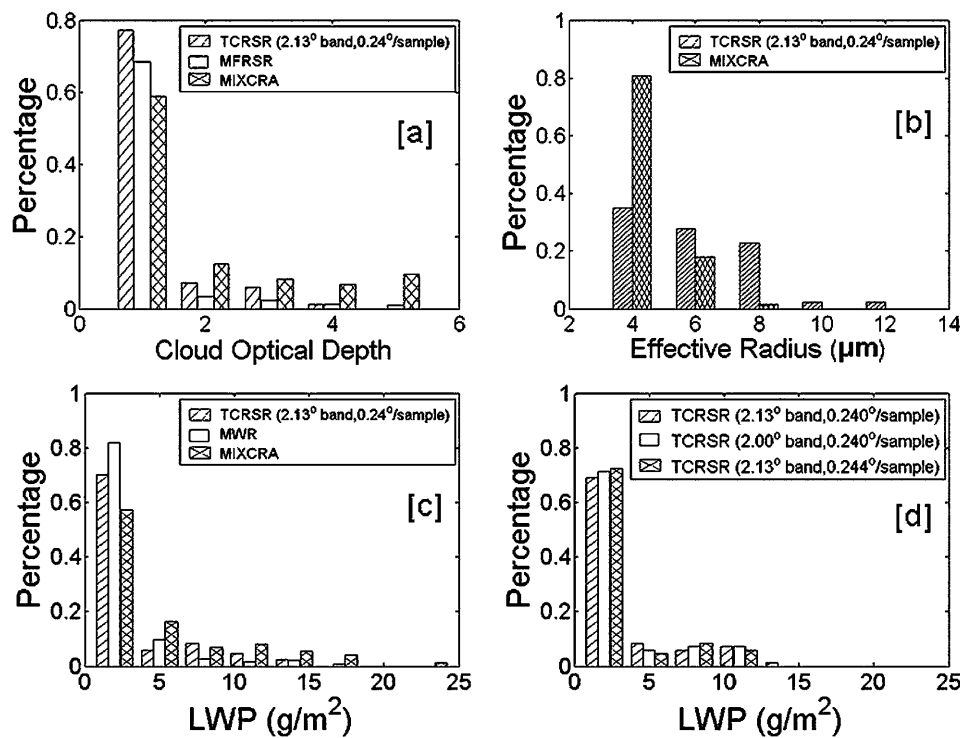


Figure 9. (a) Distributions of COD from MFRSR, AERI, and TCRSR; (b) distributions of cloud DER from AERI and TCRSR; (c) distributions of LWP from MWR, AERI, and TCRSR for cases on 3 July 2008 at the ACRF SGP site; and (d) distributions of LWP for various sensitivity tests.

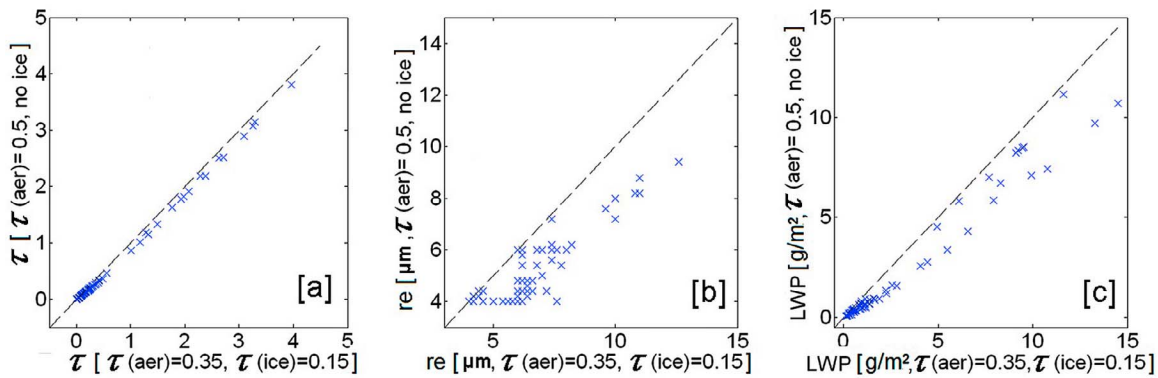


Figure 10. Comparison of the (a) retrieved COD, (b) cloud DER, and (c) cloud LWP on 3 July 2008, assuming that the ice cloud did not exist (i.e., the ice COD is 0).

distribution of background ice-cloud particles and aerosols and (2) the optical depths of both. The latter are the dominant source of retrieval uncertainties. To assess the potential impact of these uncertainties, we retrieve low-level water cloud properties assuming that no ice cloud is present, that is, we set the aerosol optical depth to 0.50 and the ice COD to 0.0. As shown in Figure 10, the retrieved COD, cloud DER, and cloud LWP are all smaller without the ice-cloud layer than with it. These changes can be explained as follows. For an observed solar aureole and direct beam, because the forward scattering of aerosol is weaker than that of ice cloud, the modeled forward scattering and solar aureole shoulder are smaller for the all-aerosol (no ice-cloud) condition, resulting in a smaller retrieved water COD. A smaller retrieved water COD with a weaker solar aureole shoulder requires a smaller effective radius to match the observed solar aureole, which holds for water CODs less than 2. With this extreme assumption of no ice cloud, our sensitivity study indicates that the uncertainty in the retrieved water COD is very small, only 0.07; however, for the DER and LWP, the uncertainties are up to 21.5% and 25.5%, respectively.

4. Discussion and Summary

[21] A prototype TCRSR was successfully developed and deployed by BNL (Bartholomew et al., submitted manuscript, 2011). The TCRSR measures the angular distribution of the forward-scattering lobe of the direct solar beam (i.e., the solar aureole) through a thin cloud from which, as proposed by *Min and Duan* [2005], the COD and DER can be simultaneously retrieved. We applied the *Min and Duan's* [2005] retrieval algorithm to the measurements of the TCRSR at the SGP site. After careful calibration and pre-processing, our results indicate that the TCRSR is able to retrieve simultaneously the COD, cloud DER, and cloud LWP for the optically thin water clouds. The retrieved COD and LWP show reasonable agreement with other measurements even for this complicated situation (thin ice cloud over low-level water clouds). Because of the lack of direct measurements of cloud DER and LWP along the Sun-sensor direction and the limited duration of the TCRSR deployment, at this time, we are unable to assess further the absolute accuracy of the TCRSR retrievals. Nonetheless, differences between the retrieved cloud DER from the TCRSR and those from other measurements are apparent in some time periods.

We have discussed some error sources in terms of measurement uncertainty and retrieval algorithm assumptions. However, some other issues are worth mentioning, such as cloud spatial variability (cloud patchiness and cloud edges) and 3-D effects. The solar aureole is dominated by forward scattering (first-order scattering) of atmospheric particles. The multiple scattering makes a limited (one order of magnitude smaller) contribution. The 3-D effects associated with the cloud spatial variability or cloud patchiness have very small effects on our retrievals. However, if the solar aureole is located at the cloud edges or regions with large spatial variability, changes of COD and drop size associated with cloud edges or spatial variability may impact the solar aureole measurements of the TCRSR. This would result in asymmetries and undulations in the shoulders of the solar aureole, which would impact cloud retrievals.

[22] Through our evaluation of the TCRSR, we found several issues that should be addressed in future developments of this kind of instrument.

[23] 1. The signal-to-noise ratio (SNR) is a critical factor as the blocked radiance is obtained by differencing two large values (unshadowed irradiance minus shadowed irradiance). A high SNR ensures the accurate determination of the solar aureole shoulders and consequently the shape of the solar aureole because the values at the shoulders are very small compared to the direct-normal irradiance for small optical depths. Given the instrument design, it is relatively easy to increase SNR by widening the blocking angle; however, this increase in SNR comes at the expense of a larger blocking angle, which in turn increases retrieval errors. Thus, we need to find the occultation angle that optimizes the trade-offs between the retrieval errors from SNR and those from the use of a bigger blocking angle.

[24] 2. The stability of the rotating speed of the shadowband and the accurate registration of the blocking angle are also key factors in determining the measured shape of the solar aureole. If the diffuser size were reduced, the width of the shadowband and its radius of rotation could also be reduced. The more compact design would diminish the potential impacts of wind and torque of the shadowband weight on the motor and would, therefore, help maintain a constant speed of rotation in real environmental conditions. Furthermore, with a smaller diffuser size, the shadow cast by the band could be reduced, which would enable a higher angular resolution of the solar aureole measurements. The

higher angular resolution would enable better cloud property retrievals.

[25] 3. A faster sweep would reduce the time needed to sample the solar aureole region and would enable retrieval of the properties of fast-moving clouds. This change would require both a faster motor and a faster detector with adequate SNR.

[26] In this article, we focused on cloud retrievals using only the 415 nm spectral band. As outlined in the study by *Min and Duan* [2005], the spectral measurements of the TCRSR can be used to retrieve aerosol optical depth and aerosol particle mean radius. This is a less challenging problem, because forward scattering for relatively small aerosol particles is not as strongly peaked as for cloud droplets. We will exploit the capability of the TCRSR in the near future to retrieve aerosol optical properties.

[27] **Acknowledgments.** We thank R. M. Reynolds for his assistance in examining the sweep behavior. The data used in these analyses were from the U.S. Department of Energy's ACRF site at the SGP. This work was supported by the U.S. Department of Energy's Atmospheric System Research program (Office of Science, OBER) under contract DE-FG02-03ER63531 and by the NOAA Educational Partnership Program with Minority Serving Institutions (EPP/MSI) under cooperative agreements NA17AE1625 and NA17AE1623; contributions from M.J.B. and A.M.V. were supported by DE-AC02-98CH10886, and contributions from D.D.T. were supported by DE-FG02-08ER64538.

References

- Ackerman, T. P., and G. M. Stokes (2003), The atmospheric radiation measurement program, *Phys. Today*, *56*, 38–45, doi:10.1063/1.1554135.
- Clothiaux, E. E., T. P. Ackerman, G. G. Mace, K. P. Moran, R. T. Marchand, M. A. Miller, and B. E. Martner (2000), Objective determination of cloud heights and radar reflectivities using a combination of active remote sensors at the ARM CART sites, *J. Appl. Meteorol.*, *39*, 645–665, doi:10.1175/1520-0450(2000)039<0645:ODOCHA>2.0.CO;2.
- DeVore, J. G., A. T. Stair, A. LePage, D. Rall, J. Atkinson, D. Villanucci, S. A. Rappaport, P. C. Joss, and R. A. McClatchey (2009), Retrieving properties of thin clouds from solar aureole measurements, *J. Atmos. Oceanic Technol.*, *26*, 2531–2548, doi:10.1175/2009JTECHA1289.1.
- Dubovik, O., A. Smirnov, B. N. Holben, M. D. King, Y. J. Kaufman, T. F. Eck, and I. Slutsker (2000), Accuracy assessments of aerosol optical properties retrieved from Aerosol Robotic Network (AERONET) Sun and sky radiance measurements, *J. Geophys. Res.*, *105*, 9791–9806, doi:10.1029/2000JD900040.
- Forgan, B. W. (1988), Comment on: Bias in solar constant determination by the Langley method due to structured atmospheric aerosol, *Appl. Opt.*, *27*, 2546–2548, doi:10.1364/AO.27.002546.
- Harrison, L., and J. Michalsky (1994), Objective algorithms for the retrieval of optical depths from ground-based measurements, *Appl. Opt.*, *33*, 5126–5132, doi:10.1364/AO.33.005126.
- Harrison, L. C., J. J. Michalsky, and J. Berndt (1994), Automated multifilter rotating shadowband radiometer: An instrument for optical depth and radiation measurements, *Appl. Opt.*, *33*, 5118–5125, doi:10.1364/AO.33.005118.
- Hodkinson, J. R. (1966), Particle sizing by means of the forward scattering lobe, *Appl. Opt.*, *5*, 839–844, doi:10.1364/AO.5.000839.
- Kaufman, Y. J., A. Gitelson, A. Karnieli, E. Ganor, R. S. Fraser, T. Nakajima, S. Mattoo, and B. N. Holben (1994), Size distribution and scattering phase function of aerosol particles retrieved from sky brightness measurements, *J. Geophys. Res.*, *99*, 10,341–10,356, doi:10.1029/94JD00229.
- Knuteson, R. O., et al. (2004a), Atmospheric Emitted Radiance Interferometer. Part I: Instrument design, *J. Atmos. Oceanic Technol.*, *21*, 1763–1776, doi:10.1175/JTECH-1662.1.
- Knuteson, R. O., et al. (2004b), Atmospheric Emitted Radiance Interferometer. Part II: Instrument performance, *J. Atmos. Oceanic Technol.*, *21*, 1777–1789, doi:10.1175/JTECH-1663.1.
- Liljegren, J. C. (1994), Two-channel microwave radiometer for observations of total column precipitable water vapor and cloud liquid water path, paper presented at Fifth Symposium on Global Change Studies, Am. Meteorol. Soc., Nashville, Tenn.
- Marchand, R., T. Ackerman, E. R. Westwater, S. A. Clough, K. Cady-Pereira, and J. C. Liljegren (2003), An assessment of microwave absorption models and retrievals of cloud liquid water using clear-sky data, *J. Geophys. Res.*, *108*(D24), 4773, doi:10.1029/2003JD003843.
- Min, Q., and M. Duan (2005), Simultaneously retrieving cloud optical depth and effective radius for optically thin clouds, *J. Geophys. Res.*, *110*, D21201, doi:10.1029/2005JD006136.
- Min, Q.-L., and L. C. Harrison (1996), Cloud properties derived from surface MFRSR measurements and comparison with GOES results at the ARM SGP site, *Geophys. Res. Lett.*, *23*, 1641–1644, doi:10.1029/96GL01488.
- Min, Q.-L., E. Joseph, and M. Duan (2004), Retrievals of thin cloud optical depth from a multifilter rotating shadowband radiometer, *J. Geophys. Res.*, *109*, D02201, doi:10.1029/2003JD003964.
- Nakajima, T., M. Tanaka, and T. Yamauchi (1983), Retrieval of the optical properties of aerosols from aureole and extinction data, *Appl. Opt.*, *22*, 2951–2959, doi:10.1364/AO.22.002951.
- Spinhrne, J. D. (1993), Micro pulse lidar, *IEEE Trans. Geosci. Remote Sens.*, *31*, 48–55, doi:10.1109/36.210443.
- Turner, D. D. (2007), Improved ground-based liquid water path retrievals using a combined infrared and microwave approach, *J. Geophys. Res.*, *112*, D15204, doi:10.1029/2007JD008530.
- Turner, D. D., R. A. Ferrare, L. A. Heilman Brasseur, W. F. Feltz, and T. P. Tooman (2002), Automated retrievals of water vapor and aerosol profiles from an operational Raman lidar, *J. Atmos. Oceanic Technol.*, *19*, 37–50, doi:10.1175/1520-0426(2002)019<0037:AROWVA>2.0.CO;2.
- Turner, D. D., et al. (2007), Thin liquid water clouds: Their importance and our challenge, *Bull. Am. Meteorol. Soc.*, *88*, 177–190, doi:10.1175/BAMS-88-2-177.
- M. J. Bartholomew and A. M. Vogelmann, Brookhaven National Laboratory, Mail Stop 490D, Upton, NY 11973, USA.
- M. Duan, Laboratory for Middle Atmosphere and Global Environment Observation, Institute of Atmospheric Physics, Chinese Academy of Sciences, Beijing 100029, China.
- Q. Min and B. Yin, Atmospheric Science Research Center, State University of New York at Albany, 251 Fuller Rd., Albany, NY 12203, USA. (min@asrc.albany.edu)
- D. D. Turner, National Severe Storms Laboratory, NOAA, 120 David L. Boren Blvd., Norman, OK 73072, USA.